



Cite this: *Nanoscale*, 2025, **17**, 9197

## Ultrasensitive detection of 2,4-dichlorophenoxyacetic acid by inhibiting alkaline phosphatase immobilized onto a highly porous gold nanocoral electrode†

Angelo Tricase,<sup>‡a,b</sup> Michele Catacchio,<sup>‡a,b</sup> Verdiana Marchianò<sup>a,b</sup>  
 Eleonora Macchia,<sup>†a,b,c</sup> Paolo Bollella<sup>†a,b,d</sup> and Luisa Torsi<sup>†b,d</sup>

Herein, we describe the design and implementation of an ultrasensitive enzyme inhibition-based biosensor for 2,4-dichlorophenoxyacetic acid (2,4-D) detection. The biosensor utilizes alkaline phosphatase (AIP), immobilized on a photo-crosslinked polymer matrix of poly(vinyl alcohol) functionalized with *N*-methyl-4(4'-formylstyryl)pyridinium (PVA-SbQ), supported by electrodes coated with highly porous gold nanocorals (hPGNCs). After preliminary electrochemical and morphological characterization, the PVA-SbQ/AIP/hPGNC electrode was tested for inhibition studies employing ascorbate 2-phosphate (A2P) as the initial substrate. The biosensor preparation/sensing time from electrode preparation to final results is approximately 45 minutes, which enables the possibility to easily scale up the electrode production process on a daily basis with a reliable analytical result in only 5 minutes of amperometric measurement. Following the initial kinetic studies and evaluation of analytical performance, the PVA-SbQ/AIP/hPGNC platform demonstrated a linear detection range from 0.002 to 22 ppt, with a sensitivity of  $0.121 \pm 0.006$  ppt<sup>-1</sup> (RSD = 4.9%,  $R^2 = 0.996$ , and  $N = 6$ ) and a limit of detection (LoD) of 0.7 ppq. This sensitivity is 7–8 orders of magnitude below the regulatory thresholds in Europe and the USA. Furthermore, the biosensor was validated using 19 homogenized wheat leaf sample extracts, prepared in line with European Food Safety Authority (EFSA) guidelines, achieving average recoveries exceeding 96% and RSD values under 9.8%. The biosensor also exhibited robust operational and storage stability, maintaining 84% (30 hours of continuous operation) and 94% (120 days) of its initial response, respectively. These results highlight the potential of the PVA-SbQ/AIP/hPGNC biosensor for on-site 2,4-D monitoring in agricultural crops and its feasibility for integration with artificial intelligence for advanced diagnostics.

Received 19th November 2024,  
 Accepted 26th February 2025

DOI: 10.1039/d4nr04857a

rsc.li/nanoscale

## 1. Introduction

2,4-Dichlorophenoxyacetic acid (2,4-D) is an herbicide acting as a growth regulator, primarily used to control broadleaf weeds in cereal crops.<sup>1–3</sup> The presence of 2,4-D residues in food and the environment presents serious health risks to humans and animals.<sup>4–6</sup> To reduce these risks, the US Environmental Protection Agency (EPA) has set a maximum contaminant level (MCL) for 2,4-D at 0.07 mg L<sup>-1</sup> (70 ppb).<sup>7,8</sup>

Based on the European Regulation (EC) no 1107/2009, further revised in the Commission Implementing Regulation (EU) 2015/2033, the Theoretical Maximum Daily Intake (TMDI) of 2,4-D for all considered consumer groups is estimated to be 3.2% of the Acceptable Daily Intake (ADI, 0.02 mg per kg body weight per day), namely 0.64 ppb.<sup>9,10</sup> Therefore, developing an effective and quick method for detecting 2,4-D is vital for ensuring the safety of food and the environment.<sup>11,12</sup>

Several traditional analytical techniques have been used to detect 2,4-D and other environmental contaminants.<sup>13,14</sup> While these methods offer high sensitivity, selectivity, and specificity, they exhibit several limitations, including the need for expensive equipment, complex sample processing, and specialized expertise.<sup>15,16</sup> Additionally, these conventional approaches are not ideal for on-site pollutant monitoring. Notably, there has been growing focus on developing alternative analytical tools that minimize sample preparation, reduce costs, shorten analysis time, and enable on-site measurements.<sup>17–19</sup>

<sup>a</sup>Department of Pharmacy-Pharmaceutical Sciences, University of Bari Aldo Moro, Via E. Orabona, 4-70125 Bari, Italy

<sup>b</sup>Centre for Colloid and Surface Science, University of Bari Aldo Moro, Via E. Orabona, 4-70125 Bari, Italy. E-mail: paolo.bollella@uniba.it

<sup>c</sup>Faculty of Science and Engineering, Åbo Akademi University, 20500 Turku, Finland

<sup>d</sup>Department of Chemistry, University of Bari Aldo Moro, Via E. Orabona, 4-70125 Bari, Italy

†Electronic supplementary information (ESI) available: Experimental section including Materials and methods. See DOI: <https://doi.org/10.1039/d4nr04857a>

‡These authors contributed equally.



Biosensors are increasingly recognized for their potential in environmental monitoring. Several enzyme- and antibody-based biosensors have been created for detecting 2,4-D, using various transducer technologies (e.g., electrochemical, surface plasmon resonance (SPR), optical methods, etc.).<sup>20–23</sup> Despite their effectiveness, these biosensors often face challenges, including the instability of antibodies and enzymes under certain conditions. More recently, electrochemical sensors using molecularly imprinted polymers (MIPs) have shown significant promise, as the imprinted materials offer improved mechanical and chemical stability.<sup>24–26</sup> Furthermore, biosensors employing whole cells, like *Pseudomonas putida* and *Anabaena torulosa*, have been developed for detecting 2,4-D.<sup>27</sup> Enzyme inhibition-based biosensors are particularly suitable for *in situ* and continuous environmental analysis.<sup>28–33</sup> These biosensors allow the study of the kinetics of the inhibition process, which requires modifications to conventional theories and equations to account for heterogeneous phases. It is also important to recognize that many biosensor signals represent transient and/or local equilibria, which may not align with traditional enzyme-based models, and enable the quantification of inhibitor concentrations by assessing the percentage of inhibition on the immobilized biocatalysts.<sup>34,35</sup>

Over the past two decades, numerous studies have focused on developing inhibition-based biosensors for detecting environmental pollutants.<sup>36,37</sup> For instance, several ALP-based biosensors have been developed for the detection of 2,4-D by measuring the inhibition of ALP activity, providing a rapid and sensitive detection method.<sup>24,25</sup> Additionally, a biosensor combining ALP with glucose oxidase has been reported for 2,4-D detection, enhancing sensitivity through a dual-enzyme approach.<sup>38</sup> Another study has developed a biosensor for detecting both 2,4-D and malathion using ALP and substrates like 3-indoxyl phosphate, phenyl phosphate, or ascorbate-2-

phosphate, demonstrating versatility in detecting multiple pollutants.<sup>39–41</sup> Furthermore, Sok *et al.* explored the use of carbon nano-onion peroxidase composite biosensors for the electrochemical detection of 2,4-D and 2,4,5-trichlorophenoxyacetic acid (2,4,5-T), highlighting advancements in nano-material-based biosensors.<sup>42</sup>

This study reports for the first time the development of an ultrasensitive enzyme inhibition-based biosensor for 2,4-D detection, where alkaline phosphatase (ALP) was entrapped through a photo-crosslinked polymer, namely poly(vinyl alcohol), *N*-methyl-4(4'-formylstyryl)pyridinium (PVA-SbQ), onto highly porous gold nanocoral (hPGNC) modified electrodes. After preliminary electrochemical and morphological characterization, the PVA-SbQ/ALP/hPGNC electrode was tested for inhibition studies employing ascorbate 2-phosphate (A2P) as the initial substrate. As reported in Fig. 1, the biosensor preparation/sensing time from electrode preparation to final results is approximately 45 minutes, which enables the possibility to easily scale up the electrode production process on a daily basis with a reliable analytical result in only 5 minutes of amperometric measurement. Finally, the biosensor was applied to detect 2,4-D in spiked wheat leaf extract samples.

## 2. Results and discussion

### 2.1 Electrochemical and morphological characterization of a highly porous gold nanocoral (hPGNC) electrode

To demonstrate the improvements of our electrodeposition method, the real electroactive area ( $A_{\text{real}}$ ) was determined by integrating the peak current associated with the reduction of gold oxide (approximately +0.9 V) during cyclic voltammetry (CV) in 0.5 M  $\text{H}_2\text{SO}_4$  at a scan rate of 100  $\text{mV s}^{-1}$ , as shown in Fig. 2A. The theoretical charge density for the reduction of gold oxide was considered to be  $390 \pm 10 \mu\text{C cm}^{-2}$ .<sup>43</sup> As a result, the  $A_{\text{real}}$  value of the hPGNC modified electrodes was  $9.58 \pm 0.63 \text{ cm}^2$  (Fig. 2A, red curve), which is approximately 96 times greater than that of the bare screen-printed gold electrodes ( $0.1 \pm 0.02 \text{ cm}^2$ , Fig. 2A black curve). The roughness factor ( $\rho$ ) could be estimated as  $76.3 \pm 5.1$  with respect to the geometric area of the screen-printed gold electrode (notably  $0.1256 \text{ cm}^2$ ). Additionally, hPGNC modified electrodes were analysed at varying scan rates (Fig. 2B) to calculate the electroactive area ( $A_{\text{ea}}$ ), roughness factor ( $\rho$ ), and electron transfer rate constant ( $k^0$ ,  $\text{cm s}^{-1}$ ).<sup>44</sup> The hPGNC modified electrodes exhibited an  $A_{\text{ea}}$  value of  $16.2 \pm 1.2 \text{ cm}^2$ , a roughness factor of  $128.9 \pm 9.5$  (derived by dividing the electroactive area by the geometric area), and an electron transfer rate constant of  $(3.2 \pm 0.2) \times 10^{-2} \text{ cm s}^{-1}$ . The electroactive area was calculated using the Randles-Ševčík equation.<sup>45</sup> The electron transfer rate constants ( $k^0$ ,  $\text{cm s}^{-1}$ ) were estimated through a combined approach incorporating the Klingler-Kochi method and the Nicholson and Shain method for both irreversible and reversible systems.<sup>46</sup> Similar to other highly porous nanostructured electrode surfaces,  $A_{\text{ea}}$  was higher than  $A_{\text{real}}$  due to the



Paolo Bollella

Paolo Bollella is an expert in electrochemical biosensors based on bio-nanomaterials. He earned his BSc (2012) and MSc (2014) degrees in Analytical Chemistry at Sapienza University of Rome and a PhD (2017) in Pharmaceutical Sciences. He worked at Clarkson University (USA) and became a Research Assistant Professor in 2019. Since 2020, he has been at the University of Bari Aldo Moro, becoming a Tenure Track

Assistant Professor in 2023. Being an author of 110 publications (H-index 34), he has received multiple awards and leads major research projects. He is an advisor at DirectSens and among the top 2% most influential scientists (Stanford ranking).



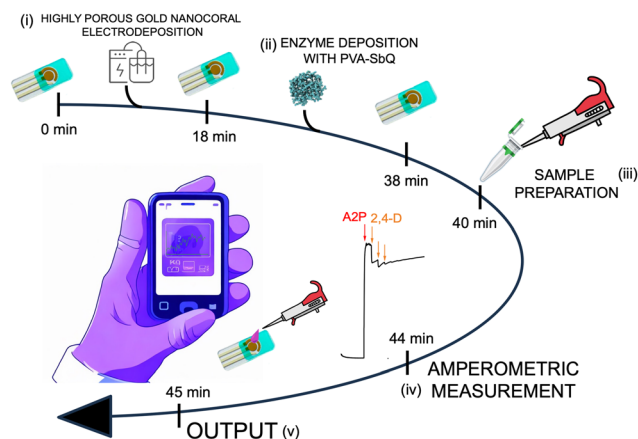


**Fig. 1** Schematic representation of the preparation/sensing time: (i) highly porous gold nanocoral electrodeposition (hPGNC), (ii) alkaline phosphatase (AIP) immobilization with UV-Vis at  $\lambda = 405$  nm in the presence of *N*-methyl-4(4'-formylstyryl)pyridinium (PVA-SbQ) as a photocrosslinked polymer, (iii) sample preparation encompassing the addition of ascorbate 2-phosphate (A2P) as an initial substrate, (iv) amperometric measurement of enzyme inhibition, and (v) final output.

complex nanostructuring occurring at the edge of the highly porous structure. The structure porosity correlates also with the rate of hydrogen bubble production during the pulsed electrodeposition steps, affecting the morphology of the electrode surface.<sup>20,47</sup>

SEM analysis was conducted to examine the morphology of the hPGNC substrates. As shown in Fig. 2C, the surfaces

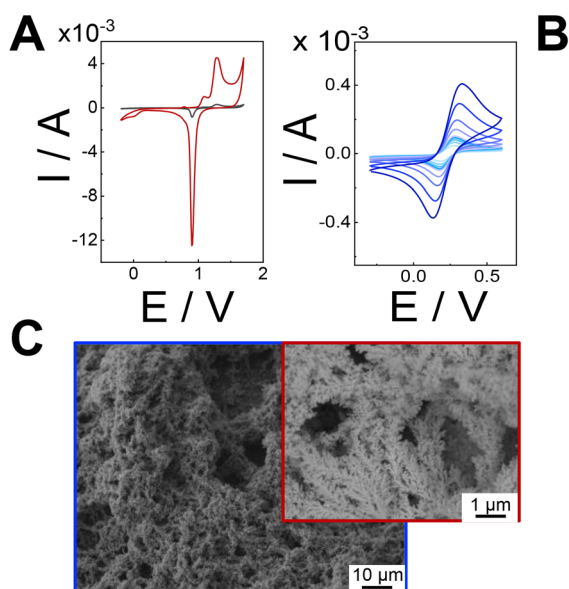


**Fig. 2** (A) CVs of the bare gold screen printed electrode (black) and the hPGNC modified electrode (red) in 0.5 M  $\text{H}_2\text{SO}_4$ . Scan rate:  $100 \text{ mV s}^{-1}$ . (B) CVs of the hPGNC modified electrode in 5 mM  $[\text{Fe}(\text{CN})_6]^{3-/4-}$  in 10 mM HEPES buffer pH 7 (containing 100 mM  $\text{Na}_2\text{SO}_4$  as a supporting electrolyte) at increasing scan rates (colour coded) in the range  $5\text{--}300 \text{ mV s}^{-1}$ . (C) SEM images of the hPGNC modified electrode.

coated with hPGNC reveal a multimodal pore size distribution, with defined pores having diameters ranging from 1 to 5  $\mu\text{m}$ , not homogeneously distributed onto the whole electrode surface. Moreover, the fine pore structure revealed the presence of coral-like nanostructures, hereinafter defined as nanocorals, with an average size of 50–200 nm.

hPGNC electrodes have been characterized through XPS analysis at each electrodeposition step: only cyclic voltammetry (CV, sample 1), cyclic voltammetry and pulsed amperometry (CV + pA, sample 2) and only pA (sample 3), as reported in Fig. S1 (ESI<sup>†</sup>). The high-resolution spectra of the gold bare electrode and hPGNC show characteristic peaks for the Au 4f signal. The expected Au 4f<sub>7/2</sub> binding energy (BE) is  $83.8 \pm 0.5$  eV, which was observed for the bare gold electrode and CV modified electrode (sample 1), indicating minimal surface changes.<sup>48</sup> However, a slight increase in the gold content and a decrease in the carbon and oxygen contents were noted (Table S1<sup>†</sup>). Significant changes occur in CV + pCA and pCA electrodes. These samples exhibit a noticeable shift in the gold signal due to pore formation, with the BE increasing to  $84.7 \pm 0.5$  eV. The gold atomic percentage also rises significantly, reaching  $59 \pm 5\%$  in sample 2 and  $62 \pm 5\%$  in sample 3 (Table S1<sup>†</sup>), but the latter experiences greater surface degradation.

Valence Band (VB) analysis, particularly near the Fermi level, confirms this shift, which is attributed to the quantum confinement effect.<sup>49</sup> The formation of nanocorals alters the electronic structure, affecting electron energy levels. The confined dimensions of nanocorals influence electron behavior, while interactions between surface atoms and metal electrons further modify their energy states.<sup>50</sup>

## 2.2 Kinetic characterization of the PVA-SbQ/AIP/hPGNC electrode

Afterwards, CV experiments were performed in 10 mM HEPES buffer pH 7 (containing 1 mM  $\text{MgSO}_4$  as a cofactor and 100 mM  $\text{Na}_2\text{SO}_4$  as a supporting electrolyte) to evaluate the enzymatic efficiency in the catalytic conversion of A2P in ascorbic acid (AA). Fig. 3A reports the catalytic CV (red dashed curve) in the presence of 2 mM AA showing an onset potential ( $E_{\text{ONSET}}$ ) of  $-0.17$  V (comparatively lower than that of the bare gold electrode, reported at 0 V) with a maximum current peak of  $36.4 \pm 2.7$  at  $+0.22$  V. Conversely, the catalytic CV (red solid curve) in the presence of 2 mM A2P shows an  $E_{\text{ONSET}}$  of  $+0.010$  V with a maximum current peak of  $11.2 \pm 0.9$  at  $+0.31$  V. The shift in the current peak potential might be ascribed to the interfacial kinetics and diffusion limitations occurring at the enzyme/electrode interface during the conversion of A2P to AA.<sup>51</sup>

Fig. 3B reports the amperometric curve (black curve) recorded for the PVA-SbQ/AIP/hPGNC electrode by applying  $E = +0.35$  V with the sequential addition of A2P in the concentration range 10–4000  $\mu\text{M}$  (control experiments are reported for the PVA-SbQ/hPGNC electrode in the presence of AA (blue curve) and A2P (orange curve)). The amperometric curve was



further fitted according to the Michaelis–Menten equation, as follows (eqn (1)):

$$I = \frac{I_{\max}c^*}{K_M + c^*} = \frac{nFA\Gamma k_{\text{cat}}c^*}{K_M + c^*} \quad (1)$$

where  $K_M$  is the Michaelis–Menten constant,  $k_{\text{cat}}$  is the turnover constant for A2P conversion to AA,  $\Gamma$  is the enzymatic surface coverage (namely AIP),  $c^*$  is the substrate concentration (namely A2P) and  $I_{\max}$  is the maximum catalytic current, while  $n$ ,  $F$  and  $A$  have their usual meaning. Fig. 3C depicts the fitted curve (black line) based on the data extracted from the amperometric output (Fig. 3B) represented as a scattered plot, resulting in a  $K_M$  value of  $78.9 \pm 3.6 \mu\text{M}$  and an  $I_{\max}$  value of  $3.6 \pm 0.1 \mu\text{A}$  ( $R^2 = 0.982$ ). The  $k_{\text{cat}}$  was computed as  $0.22 \pm 0.01 \text{ s}^{-1}$

(obtained considering an enzymatic surface coverage of  $8.5 \text{ pmol cm}^{-2}$  estimated through the p-NPP enzymatic assay) and a  $k_{\text{cat}}/K_M$  value of  $2788 \text{ s}^{-1} \text{ M}^{-1}$ . All enzymatic parameters estimated through the amperometric data agree with other results reported in the literature.<sup>39,40</sup>

After preliminary enzymatic characterization, the PVA-SbQ/AIP/hPGNC electrode was further assessed by performing amperometric experiments in the presence of A2P as a substrate (indicated with red arrows) followed by the addition of sequential concentration of 2,4-dichlorophenoxyacetic acid (2,4-D, orange arrows) in the range  $1 \text{ fM}$  ( $1 \times 10^{-15} \text{ M}$ ) to  $2 \text{ mM}$  ( $2 \times 10^{-3} \text{ M}$ ) as an analytical target (acting as an inhibitor of the AIP enzymatic activity, Fig. 3D), and 2,4,5-trichlorophenoxyacetic acid (2,4,5-T) as a negative control. The calibration

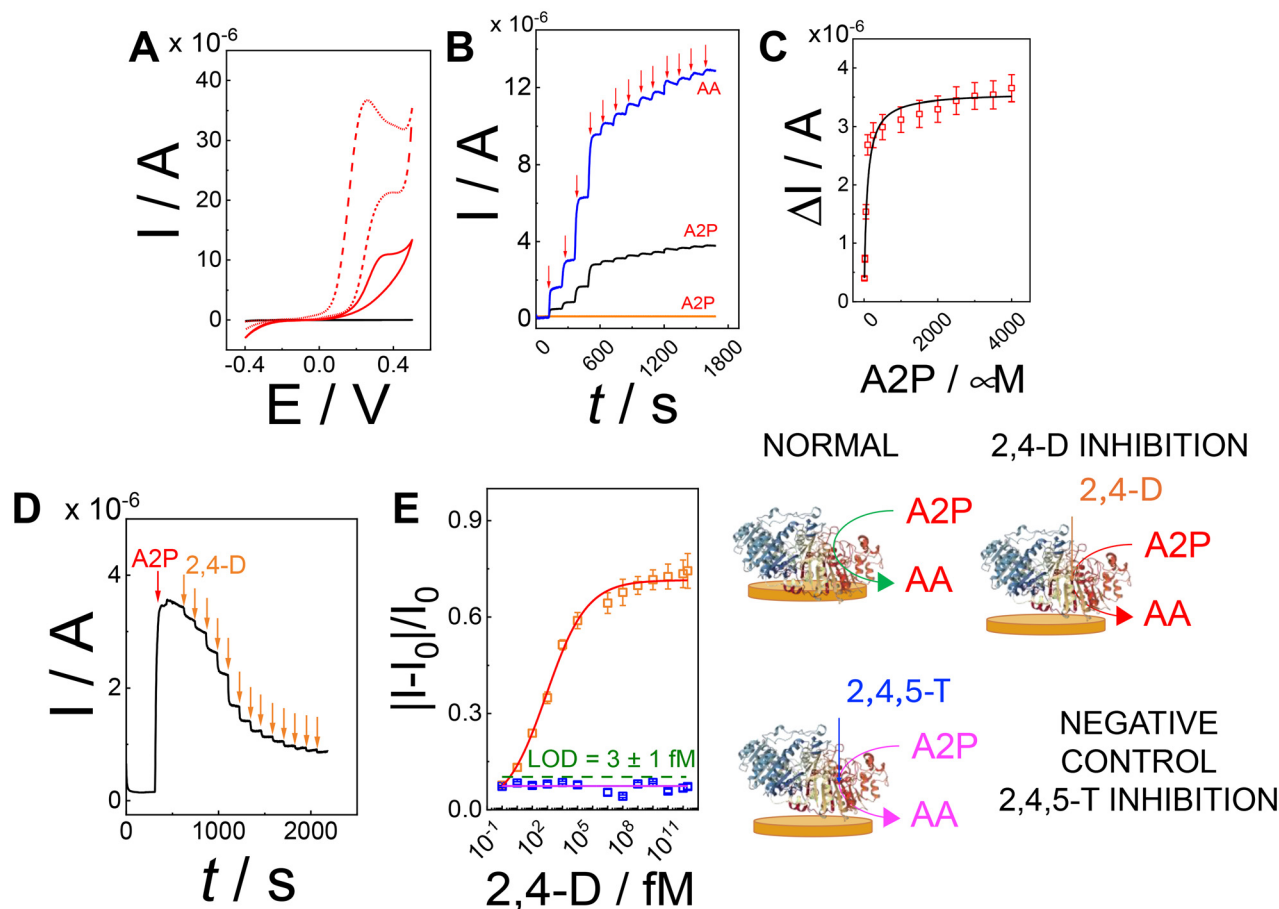


**Fig. 3** (A) CVs of the PVA-SbQ/AIP/hPGNC electrode in 10 mM HEPES buffer pH 7 (containing 1 mM  $\text{MgSO}_4$  as a cofactor and 100 mM  $\text{Na}_2\text{SO}_4$  as a supporting electrolyte, black curve) with the addition of 2 mM AA (red dashed curve) and 2 mM A2P (red solid curve) recorded at  $5 \text{ mV s}^{-1}$ . (B) The amperometric curve of the PVA-SbQ/AIP/hPGNC electrode recorded by applying  $E = +0.35 \text{ V}$  and adding A2P in the concentration range  $10\text{--}4000 \mu\text{M}$  every 100 s (black curve); the PVA-SbQ/hPGNC electrode recorded by applying  $E = +0.35 \text{ V}$  and adding AA (blue curve) and A2P (orange curve) in the concentration range  $10\text{--}4000 \mu\text{M}$  every 100 s. Addition of AA and A2P (red arrows). (C) Calibration plot of the PVA-SbQ/AIP/hPGNC electrode with Michaelis–Menten fitting (black curve) for data extracted from the amperometric curve recorded by applying  $E = +0.35 \text{ V}$  and adding A2P in the concentration range  $10\text{--}4000 \mu\text{M}$ . (D) The amperometric curve of the PVA-SbQ/AIP/hPGNC electrode recorded by applying  $E = +0.35 \text{ V}$  and adding 2 mM A2P (red arrow) as a substrate, and 2,4-D in the concentration range  $1 \text{ fM}$  ( $1 \times 10^{-15} \text{ M}$ ) to  $2 \text{ mM}$  ( $2 \times 10^{-3} \text{ M}$ ) (orange arrows) as an inhibitor, every 100 s. (E) Calibration plot of the PVA-SbQ/AIP/hPGNC electrode with Hill fitting applied to the mixed inhibition model for data extracted from the amperometric curve of the PVA-SbQ/AIP/hPGNC electrode recorded in the presence of 2,4-D in the concentration range  $1 \text{ fM}$  ( $1 \times 10^{-15} \text{ M}$ ) to  $2 \text{ mM}$  ( $2 \times 10^{-3} \text{ M}$ ) (orange dots, red fitting line) and 2,4,5-T in the same concentration range as a negative control (blue dots and magenta fitting line); insets: schematic representation of the catalytic process and inhibition process occurring at the AIP modified electrode.



curves of PVA-SbQ/AlP/hPGNC for both 2,4-D (orange dots, red fitted line) and 2,4,5-T (blue dots, magenta fitted line) are reported in Fig. 3E and fitted with the Hill equation. Recently, AlP was reported to exhibit a mixed inhibition. In this model, the inhibitor can bind to both the enzyme–substrate complex and the free enzyme, but with different affinities, making the inhibition both competitive (affecting the substrate binding) and non-competitive (affecting the AlP activity). The Hill equation for mixed inhibition is an extension of the Michaelis–Menten equation that accounts for both competitive and non-competitive inhibition, with the added consideration of cooperativity.<sup>25</sup>

In the case of mixed inhibition, the inhibitor binds to both the free AlP and the AlP-A2P complex, but with different affinities. This can be described using the following equation (eqn (2)):

$$I = \frac{I_{\max}(c^*)^n}{K_M \left(1 + \frac{c_1^*}{K_I}\right) + c^* \left(1 + \frac{c_1^*}{K_I'}\right)^n} \quad (2)$$

where  $c_1^*$  is the inhibitor concentration,  $K_I$  is the inhibition constant for the free AlP (competitive inhibition part),  $K_I'$  is the inhibition constant for the AlP-A2P complex (non-competitive inhibition part), and  $n$  is the Hill coefficient (reflects cooperativity of the AlP-A2P interaction), while  $K_M$ ,  $I_{\max}$ , and  $c^*$  have their usual meaning. Hence,  $K_I$  and  $K_I'$  are  $827 \pm 98$  fM and  $785 \pm 63$  fM, respectively, while the Hill coefficient ( $n$ ) is  $0.32 \pm 0.01$  ( $R^2 = 0.997$  and  $N = 6$ ). In this case, the PVA-SbQ/AlP/hPGNC electrode exhibited negative cooperativity, where the binding of 2,4-D molecules reduced the affinity of AlP for additional A2P molecules. Similarly, the same fitting model was applied to 2,4,5-T inhibition showing no inhibiting response on AlP.

### 2.3 Analytical characterization of the PVA-SbQ/AlP/hPGNC electrode

Furthermore, the calibration curve reported in Fig. 3E reported a limit of detection (LoD) of  $3 \pm 1$  fM calculated as  $\bar{x}_B + 3\sigma_B$ , considering the average current response reported for 2,4,5-T as a negative control. The calibration curve exhibited a linear range between 10 fM ( $1 \times 10^{-15}$  M) and 100 pM ( $100 \times 10^{-12}$  M), with a sensitivity of  $0.121 \pm 0.006$  fM<sup>-1</sup> (RSD = 4.9%,  $R^2 = 0.996$ , and  $N = 6$ , Fig. 4A). Using the calibration curve, the LoD can be estimated as follows (eqn (3)):

$$\text{LoD} = \frac{3\sigma_B}{m} \quad (3)$$

where  $\sigma_B$  is the standard deviation of the blank response (current measured for 2,4,5-T as a negative control) and  $m$  is the slope of the calibration curve. The calculated LoD for the PVA-SbQ/AlP/hPGNC electrode was  $3.2 \pm 1.1$  fM. Since 2,4-D is a contaminant, the MRLs and threshold are reported according to parts-per notation. Hence, the linear range was calculated in the range 0.002–22 ppt, with a sensitivity of  $0.121 \pm 0.006$  ppt<sup>-1</sup> (RSD = 4.9%,  $R^2 = 0.996$ , and  $N = 6$ ) and a LoD of

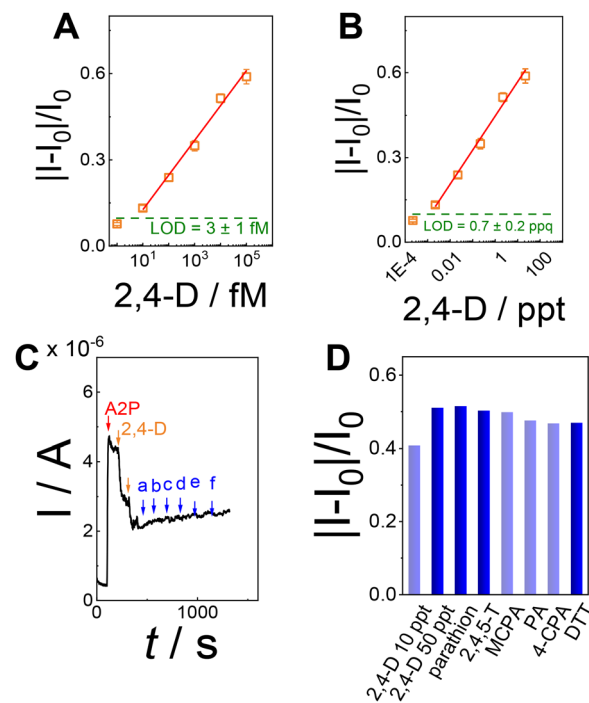


**Fig. 4** (A) Linear range extracted from the calibration plot for the PVA-SbQ/AlP/hPGNC electrode recorded in the presence of 2,4-D in the concentration range 1 fM ( $1 \times 10^{-15}$  M) to 2 mM ( $2 \times 10^{-3}$  M) (orange dots, red fitting line); the linear range between 10 fM ( $1 \times 10^{-15}$  M) and 100 pM ( $100 \times 10^{-12}$  M). (B) The linear range reported to be in the range 0.002–22 ppt of 2,4-D for the PVA-SbQ/AlP/hPGNC electrode. (C) The amperometric curve to test the interfering compounds by adding 10 and 50 ppt of 2,4-D (in the presence of A2P as a substrate) and testing sequentially (a) parathion, (b) 2,4,5-T, (c) MCPA, (d) PA, (e) 4-CPA and (f) DDT at a concentration of 100 ppt. Experimental parameters:  $E = +0.35$  V; A2P 2 mM. (D) Bar diagram for amperometric responses of the PVA-SbQ/AlP/hPGNC electrode in the presence of (a) parathion, (b) 2,4,5-T, (c) MCPA, (d) PA, (e) 4-CPA and (f) DDT at a concentration of 100 ppt.

0.7 ppq (Fig. 4B), which is 7–8 orders of magnitude lower than the law limit established in both Europe and the USA.<sup>8,52</sup>

The selectivity of PVA-SbQ/AlP/hPGNC was investigated by adding 1 and 10 ppt of 2,4-D (in the presence of A2P as a substrate) and testing sequentially 100 ppt of potentially inhibiting pesticides, as reported in Fig. 4C. The bar diagram (Fig. 4D) shows a 5–7% decrease in the response for parathion, 2,4,5-T and MCPA because organophosphate pesticides can act as AlP inhibitors, while for 2,4,5-T and MCPA, there is a minimal structural difference.<sup>26</sup> Similarly, PA, 4-CPA and DDT show a decrease of 8–9% in the analytical signal, due to the structural similarity (most of the inhibiting function occurs at the level of the aromatic ring interacting with the AlP active site), while DDT is a well-known organochlorine pesticide, and similar to other organochlorine compounds, it has been shown to have toxic effects on various biological systems, including enzyme inhibition.<sup>53</sup>

The effects of temperature and pH are depicted in Fig. 5A and B, respectively. Regarding temperature dependence, the



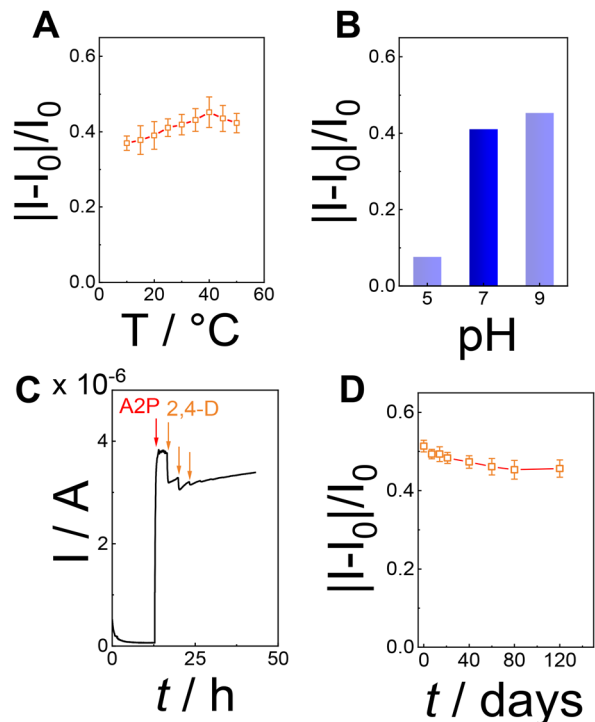


**Fig. 5** (A) Temperature effect measured for the PVA-SbQ/AIP/hPGNC electrode in the presence of 10 ppt 2,4-D. Experimental parameters:  $E = +0.35$  V; A2P 2 mM. (B) Bar diagram of the pH effect measured for the PVA-SbQ/AIP/hPGNC electrode in the presence of 10 ppt 2,4-D. Experimental parameters:  $E = +0.35$  V; A2P 2 mM. (C) Operational stability of the PVA-SbQ/AIP/hPGNC electrode measured over 30 hours of continuous measurements after the addition of 1 and 10 ppt 2,4-D; experimental parameters:  $E = +0.35$  V; A2P 2 mM. (D) Storage stability of the PVA-SbQ/AIP/hPGNC electrode measured in the presence of 10 ppt 2,4-D over 120 days; experimental parameters:  $E = +0.35$  V; A2P 2 mM.

PVA-SbQ/AIP/hPGNC electrode demonstrated the best performance at 40 °C. However, the biosensor maintained good activity at both room temperature and 40 °C. Above 40 °C, the current density dropped, likely due to enzyme denaturation. The optimal pH was found to be 9 in a 10 mM Tris buffer, which aligns with other AIP-inhibition biosensors. However, the catalytic response is comparable also at pH 7 in a 10 mM HEPES buffer (decreasing by 12%), while the current output decreased sharply at acidic pH, which agrees with previous literature findings.<sup>24,25</sup>

The operational stability of PVA-SbQ/AIP/hPGNC was tested in the presence of A2P as a substrate followed by two sequential additions of 2,4-D up to 10 ppt, retaining 84% of the initial response over 30 hours of continuous measurement (Fig. 5C). Additionally, the storage stability of PVA-SbQ/AIP/hPGNC was evaluated considering the current response measured for 2,4-D inhibition at 10 ppt over 120 days, retaining 94% of the initial activity (Fig. 5D).

To validate the potential of the PVA-SbQ/AIP/hPGNC electrode for the on-site detection of 2,4-D as a screening tool for analytical process control in wheat farming, the proposed biosensor was employed to measure 2,4-D concentrations in

**Table 1** Results obtained for 2,4-D spiked wheat leaf sample extract analysed with the PVA-SbQ/AIP/hPGNC electrode (SD values are reported for each sample)

Sample ID	Found value/ppt	Nominal value/ppt	Recovery %
#1001	1.02 ± 0.11	1	102
#1002	9.74 ± 0.18	10	97.4
#1003	0.08 ± 0.01	0.1	80
#1004	0.92 ± 0.09	1	92
#1005	0.09 ± 0.01	0.1	90
#1006	0.08 ± 0.01	0.1	80
#1007	0.91 ± 0.13	1	91
#1008	0.88 ± 0.14	1	88
#1009	0.95 ± 0.11	1	95
#1010	10.42 ± 0.18	10	104.2
#1011	0.09 ± 0.01	0.1	90
#1012	10.11 ± 0.21	10	101
#1013	1.18 ± 0.18	1	118
#1014	0.11 ± 0.01	0.1	110
#1015	9.82 ± 0.21	10	98
#1016	1.12 ± 0.19	1	112
#1017	1.08 ± 0.25	1	108
#1018	0.09 ± 0.01	0.1	90
#1019	0.08 ± 0.01	0.1	80

19 homogenized wheat leaf sample extracts collected and processed following the procedure outlined in the European Food Safety Authority (EFSA) guidelines.<sup>54</sup> The real wheat samples, labelled (numerical order) and collected from different local farms, were spiked with 3 different concentrations of 2,4-D, namely 0.1, 1 and 10 ppt, as reported in Table 1.

The proposed biosensor demonstrates good performance across all homogenized wheat leaf samples, with average recovery values of 88.6% (RSD <11.4% calculated based on average recovery values) for 0.1 ppt, 100.8% (RSD <12.4% calculated based on average recovery values) for 1 ppt, 100.2% (RSD <3.5% calculated based on average recovery values) for 10 ppt 2,4-D spiked wheat sample extract, respectively. Moreover, the average recovery is above 96% with an RSD below 9.8%, proving the ability of the PVA-SbQ/AIP/hPGNC electrode to reliably measure 2,4-D in farming samples. The proposed biosensor PVA-SbQ/AIP/hPGNC was compared with other platforms reported in the literature reporting the lowest LoD, high sensitivity, and longer operational and storage stability (Table S2†).<sup>28,55–58</sup>

### 3. Conclusions

This study reports the development of an ultrasensitive enzyme inhibition-based biosensor for detecting 2,4-D, where alkaline phosphatase (AIP) is immobilized *via* a photo-crosslinked polymer, poly(vinyl alcohol)-*N*-methyl-4(4'-formylstyryl)pyridinium (PVA-SbQ), on electrodes modified with highly porous gold nanocorals (hPGNCs). After preliminary kinetics and analytical performance, the PVA-SbQ/AIP/hPGNC biosensing platform exhibited a linear range of 0.002–22 ppt, with a sensitivity of  $0.121 \pm 0.006$  ppt<sup>-1</sup> (RSD = 4.9%,  $R^2 = 0.996$  and  $N = 6$ ) and a LoD of 0.7 ppq, which is 7–8 orders of



magnitude lower than the law limit established in both Europe and the USA. Additionally, the PVA-SbQ/ALP/hPGNC electrode was tested in 19 homogenized wheat leaf sample extracts according to the European Food Safety Authority (EFSA) guidelines, reporting an average recovery above 96% with an RSD below 9.8%. The proposed biosensor also showed good operational and storage stability retaining 84% (30 hours of continuous operation) and 94% of the initial response (120 days), respectively. The overall analytical performance confirms the possibility of employing the PVA-SbQ/ALP/hPGNC biosensor for on-site 2,4-D analysis in farming crops and the possibility of being coupled with artificial intelligence as a diagnostic tool.

## Author contributions

A.T., M.C., and V.M. wrote a part of the manuscript. E.M., P.B. and L.T. supervised A.T. and M.C. on data collection and analysis. L.T., E.M. and P.B. conceived the experimental work, revised the manuscript and are responsible for funding acquisition. All authors approved the final version.

## Data availability

Data for this article are available at Zenodo at <https://doi.org/10.5281/zenodo.14172625>.

## Conflicts of interest

There are no conflicts to declare.

## Acknowledgements

The following funding agencies are acknowledged: NoOne-A binary sensor with a single-molecule digit to discriminate biofluids enclosing zero or at least one biomarker, ERC Stg2021, GA:101040383; Centro di Innovazione in Single-Molecule Digital Assay – “Digital Assay” from Regione Puglia DGR N. 218 of 21/02/2022; the Italian network of excellence for advanced diagnosis (INNOVA), Ministero della Salute -code PNC-E3-2022-23683266 PNC-HLS-DA, CUP: C43C22001630001; Complementary National Plan PNC-I.1 “Research initiatives for innovative technologies and pathways in the health and welfare sector” D.D. 931 of 06/06/2022, DARE – DigitAl lifelong pRevEntion initiative, code PNC0000002. This work was partially supported by the European Union – Next Generation EU under the Italian National Recovery and Resilience Plan (NRRP), Mission 4, Component 2, Investment 1.3, CUP D43C22003080001, partnership on “Telecommunications of the Future” (PE00000001 – program “RESTART”), and CSGI (Centre for Colloid and Surface Science).

## References

- 1 K. Magnoli, C. S. Carranza, M. E. Aluffi, C. E. Magnoli and C. L. Barberis, *Environ. Sci. Pollut. Res.*, 2020, **27**, 38501–38512.
- 2 V. V. Butova, T. V. Bauer, V. A. Polyakov, V. D. Rajput and T. M. Minkina, *Crop Prot.*, 2024, 106865.
- 3 J. Torra, R. Alcántara-de La Cruz, M. R. A. De Figueiredo, T. A. Gaines, M. Jugulam, A. Merotto, C. Palma-Bautista, A. M. Rojano-Delgado and D. E. Riechers, *Pest Manage. Sci.*, 2024, **80**, 6041–6052.
- 4 S.-F. Chen, W.-J. Chen, H. Song, M. Liu, S. Mishra, M. A. Ghorab, S. Chen and C. Chang, *Molecules*, 2024, **29**, 3869.
- 5 R. Mesnage and M. Antoniou, in *Herbicides*, Elsevier, 2021, pp. 143–180.
- 6 J. C. Carrizo, S. V. Duy, G. Munoz, G. Marconi, M. V. Amé and S. Sauvé, *Chemosphere*, 2022, **309**, 136769.
- 7 2,4-D; Pesticide Tolerances, <https://www.federalregister.gov/documents/2017/02/07/2017-02477/24-d-pesticide-tolerances>, (accessed November 16, 2024).
- 8 E. F. S. Authority, (EFSA), A. Brancato, D. Brocca, C. D. Lentdecker, Z. Erdos, L. Ferreira, L. Greco, S. Jarrah, D. Kardassi, R. Leuschner, C. Lythgo, P. Medina, I. Miron, T. Molnar, A. Nougadere, R. Pedersen, H. Reich, A. Sacchi, M. Santos, A. Stanek, J. Sturma, J. Tarazona, A. Theobald, B. Vagenende, A. Verani and L. Villamar-Bouza, *EFSA J.*, 2017, **15**, e04765.
- 9 Regulation - 1107/2009 - EN - EUR-Lex, <https://eur-lex.europa.eu/eli/reg/2009/1107/oj>, (accessed November 16, 2024).
- 10 *Commission Implementing Regulation (EU) 2015/2033 of 13 November 2015 renewing the approval of the active substance 2,4-D in accordance with Regulation (EC) No 1107/2009 of the European Parliament and of the Council concerning the placing of plant protection products on the market, and amending the Annex to Commission Implementing Regulation (EU) No 540/2011 (Text with EEA relevance)*, 2015, vol. 298.
- 11 M. Ortiz-Martínez, J. A. Molina González, G. Ramírez García, A. De Luna Bugallo, M. A. Justo Guerrero and E. C. Strupiechonski, *Environ. Toxicol. Chem.*, 2024, **43**, 1468–1484.
- 12 V. Kumar, K. Vaid, S. A. Bansal and K.-H. Kim, *Biosens. Bioelectron.*, 2020, **165**, 112382.
- 13 J. O. Ighalo, V. E. Ojukwu, C. T. Umeh, C. O. Aniagor, C. E. Chinyelu, O. J. Ajala, K. Dulta, A. O. Adeola and S. Rangabhashiyam, *J. Water Process Eng.*, 2023, **56**, 104514.
- 14 M. Mohammadnia, R. Heydari and M. R. Sohrabi, *J. Environ. Sci. Health, Part B*, 2020, **55**, 293–300.
- 15 F. C. Christopher, P. S. Kumar, F. J. Christopher, G. J. Joshiba and P. Madhesh, *J. Cleaner Prod.*, 2020, **269**, 122356.
- 16 B. Pérez-Fernández, A. Costa-García and A. de la E. Muñoz, *Biosensors*, 2020, **10**, 32.
- 17 A. P. Turner, *Chem. Soc. Rev.*, 2013, **42**, 3184–3196.
- 18 A. Tricase, A. Imbriano, E. Macchia, L. Sarcina, C. Scandurra, F. Torricelli, N. Cioffi, L. Torsi and P. Bollella, *Electrochem. Sci. Adv.*, 2023, **3**, e2100215.



- 19 L. Uzun and A. P. Turner, *Biosens. Bioelectron.*, 2016, **76**, 131–144.
- 20 P. Bollella, *Nanomaterials*, 2020, **10**, 722.
- 21 R. Antiochia, P. Bollella, G. Favero and F. Mazzei, *Int. J. Anal. Chem.*, 2016, **2016**, 1–15.
- 22 M. Catacchio, M. Caputo, L. Sarcina, C. Scandurra, A. Tricase, V. Marchianò, E. Macchia, P. Bollella and L. Torsi, *Faraday Discuss.*, 2024, **250**, 9–42.
- 23 S. Sasipongpana, Y. Rayanasukha, S. Prichanont, C. Thanachayanont, S. Porntheeraphat and N. Hounkamhang, *Mater. Today: Proc.*, 2017, **4**, 6458–6465.
- 24 C. Tortolini, P. Bollella, R. Antiochia, G. Favero and F. Mazzei, *Sens. Actuators, B*, 2016, **224**, 552–558.
- 25 P. Bollella, G. Fusco, C. Tortolini, G. Sanzò, R. Antiochia, G. Favero and F. Mazzei, *Anal. Bioanal. Chem.*, 2016, **408**, 3203–3211.
- 26 A. Tricase, V. Marchianò, E. Macchia, N. Ditaranto, L. Torsi and P. Bollella, *Electrochim. Acta*, 2024, **494**, 144430.
- 27 B. Ritcharoon, R. Sallabhan, N. Toewiwat, S. Mongkolsuk and S. Loprasert, *J. Microbiol. Methods*, 2020, **175**, 105997.
- 28 F. Arduini, S. Cinti, V. Caratelli, L. Amendola, G. Palleschi and D. Moscone, *Biosens. Bioelectron.*, 2019, **126**, 346–354.
- 29 F. Arduini, D. Neagu, V. Scognamiglio, S. Patarino, D. Moscone and G. Palleschi, *Chemosensors*, 2015, **3**, 129–145.
- 30 I. Cacciotti, F. Pallotto, V. Scognamiglio, D. Moscone and F. Arduini, *Mater. Sci. Eng., C*, 2020, **111**, 110744.
- 31 A. Cioffi, M. Mancini, V. Gioia and S. Cinti, *Environ. Sci. Technol.*, 2021, **55**, 8859–8865.
- 32 A. Miglione, A. Raucci, M. Mancini, V. Gioia, A. Frugis and S. Cinti, *Talanta*, 2025, **283**, 127093.
- 33 F. Silveri, F. Della Pelle, A. Scroccarello, Q. U. Ain Bukhari, M. Del Carlo and D. Compagnone, *Talanta*, 2022, **240**, 123212.
- 34 L. El Harrad, I. Bourais, H. Mohammadi and A. Amine, *Sensors*, 2018, **18**, 164.
- 35 V. Arkhypova, O. Soldatkin, A. Soldatkin and S. Dzyadevych, *Chem. Rec.*, 2024, **24**, e202300214.
- 36 A. Amine, F. Arduini, D. Moscone and G. Palleschi, *Biosens. Bioelectron.*, 2016, **76**, 180–194.
- 37 B. Bucur, F.-D. Munteanu, J.-L. Marty and A. Vasilescu, *Biosensors*, 2018, **8**, 27.
- 38 C. Botrè, F. Botrè, F. Mazzei and E. Podestà, *Environ. Toxicol. Chem.*, 2000, **19**, 2876–2881.
- 39 F. Mazzei, F. Botrè, S. Montilla, R. Pilloton, E. Podestà and C. Botrè, *J. Electroanal. Chem.*, 2004, **574**, 95–100.
- 40 L. K. Shyuan, L. Y. Heng, M. Ahmad, S. A. Aziz and Z. Ishak, *Asian J. Biochem.*, 2008, **3**, 359–365.
- 41 K.-S. Loh, Y. H. Lee, A. Musa, A. A. Salmah and I. Zamri, *Sensors*, 2008, **8**, 5775–5791.
- 42 V. Sok and A. Fragoso, *Appl. Sci.*, 2021, **11**, 6889.
- 43 S. Trasatti and O. A. Petrii, *Pure Appl. Chem.*, 1991, **63**, 711–734.
- 44 V. Marchianò, A. Tricase, M. Caputo, E. Farini, R. Leardi, A. Imbriano, D. Leech, R. Kidayaveetil, L. Gentile, L. Torsi, E. Macchia and P. Bollella, *Chem. Mater.*, 2024, **36**, 358–370.
- 45 T. R. Paixão, *ChemElectroChem*, 2020, **7**, 3414–3415.
- 46 I. Lavagnini, R. Antiochia and F. Magno, *Electroanalysis*, 2004, **16**, 505–506.
- 47 P. Bollella, Y. Hibino, K. Kano, L. Gorton and R. Antiochia, *Anal. Chem.*, 2018, **90**, 12131–12136.
- 48 E. R. Kötz, H. Neff and K. Müller, *J. Electroanal. Chem. Interfacial Electrochem.*, 1986, **215**, 331–344.
- 49 J. A. La, H. Lee, D. Kim, H. Ko and T. Kang, *Nano Lett.*, 2024, **24**, 7025–7032.
- 50 H. Li, H. Yu, X. Quan, S. Chen and Y. Zhang, *ACS Appl. Mater. Interfaces*, 2016, **8**, 2111–2119.
- 51 R. A. S. Luz, A. R. Pereira, J. C. P. De Souza, F. C. P. F. Sales and F. N. Crespilho, *ChemElectroChem*, 2014, **1**, 1751–1777.
- 52 E. F. S. Authority, *EFSA J.*, 2014, **12**, 3812.
- 53 M. Majdinasab, M. Daneshi and J. L. Marty, *Talanta*, 2021, **232**, 122397.
- 54 European Food Safety Authority, *EFSA J.*, 2017, **15**, e04982.
- 55 X. Ye, F. Zhang, L. Yang, W. Yang, L. Zhang and Z. Wang, *Talanta*, 2022, **245**, 123489.
- 56 X. Li, C. Chen, F. Xu, Z. Liang, G. Xu, F. Wei, J. Yang, Q. Hu, J. Zou and Y. Cen, *Talanta*, 2023, **260**, 124639.
- 57 D. Su, X. Han, X. Yan, R. Jin, H. Li, D. Kong, H. Gao, F. Liu, P. Sun and G. Lu, *Anal. Chem.*, 2020, **92**, 12716–12724.
- 58 A.-P. Deng and H. Yang, *Sens. Actuators, B*, 2007, **124**, 202–208.

